



Ignition and Combustion Characteristics of Al/RDX/NC Nanostructured Microparticles

Gregory Young, Daniel P. Wilson, Michael Kessler, Jeffery B. DeLisio & Michael R. Zachariah

To cite this article: Gregory Young, Daniel P. Wilson, Michael Kessler, Jeffery B. DeLisio & Michael R. Zachariah (2020): Ignition and Combustion Characteristics of Al/RDX/NC Nanostructured Microparticles, Combustion Science and Technology, DOI: [10.1080/00102202.2020.1733541](https://doi.org/10.1080/00102202.2020.1733541)

To link to this article: <https://doi.org/10.1080/00102202.2020.1733541>



Published online: 27 Feb 2020.



Submit your article to this journal [↗](#)



Article views: 75



View related articles [↗](#)



View Crossmark data [↗](#)



Ignition and Combustion Characteristics of Al/RDX/NC Nanostructured Microparticles

Gregory Young^a, Daniel P. Wilson^a, Michael Kessler^a, Jeffery B. DeLisio^b, and Michael R. Zachariah^c

^aResearch Department, Naval Surface Warfare Center Indian Head Explosive Ordnance Disposal Technology Division, Indian Head, Maryland, USA; ^bDepartment of Chemistry, University of Maryland, College Park, Maryland, USA; ^cDepartment of Chemical and Environmental Engineering, University of California, Riverside, California, USA

ABSTRACT

Nanostructured microparticles composed of nanoaluminum, 1,3,5-trinitrohexahydro-*s*-triazine (RDX), and nitrocellulose (NC) were produced using electrospray assembly and studied in an experimental investigation of their ignition and combustion characteristics. All particles contained 5% NC by weight, while the nanoaluminum content ranged from 23.75 to 85.5% by weight, with the balance being RDX. T-jump wire ignition and laser ignition experiments were conducted with pressures ranging from 0.101 to 5.17 MPa. The T-jump experiments demonstrated that the aluminum component of the particle at least partially combusted anaerobically with the combustion products of the RDX and NC. This was further verified by laser ignition experiments in an inert environment via emission spectroscopy. Broad band light emission was used during laser ignition experiments to characterize ignition delay in both air and inert environments (nitrogen or argon). Ignition delay was independent of gaseous environment suggesting that particle ignition was driven by the decomposition/combustion process of RDX and NC. Ignition delay decreased with decreasing RDX content at 0.101 MPa and decreased asymptotically with increasing pressure.

ARTICLE HISTORY

Received 16 July 2019
Revised 23 January 2020
Accepted 19 February 2020

KEYWORDS

Nanocomposite;
mesoparticle; laser Ignition

Introduction

Metallic particles are commonly used as supplemental fuel additives in propellants and explosives because of their ability to improve key performance metrics due to their high heats of combustion. Aluminum powders in particular have found wide spread use in each application due to its abundance, cost, and demonstrated ability to improve performance. Nonetheless, further performance enhancements could be realized by optimization of manufacturing techniques and combustion characteristics. The primary way to achieve the desired performance enhancements would be to increase the overall reactivity of the metallic particles which would ideally result in a reduction in ignition temperature and overall burning time.

Traditionally aluminum powder on the scale of 10's of micrometers have been used in propellant formulations which has resulted in a tremendous amount of research on

aluminum ignition and combustion dating back to the 1960's (Brzustowski and Glassman 1964; Friedman and Macek 1962, 1963). This early work identified the critical ignition temperature for aluminum particles of approximately 2000–2300 K correlating with the melting temperature of the oxide shell. As particle sizes were reduced into the nanoscale, several studies (Bazyn, Krier, Glumac 2007; Trunov et al. 2006) revealed that the ignition temperature of the particles decreased significantly. In addition, Bazyn, Krier, and Glumac (2007) found that the burning times of nanoscale aluminum particles were significantly reduced suggesting a significant overall increase in aluminum particle reactivity.

For practical use, particularly in a propellant, high solids loadings are desirable within a polymer matrix with relatively high metal content. Unfortunately, this presents a major challenge with nanomaterials because of processing constraints. Due to the high specific surface area of nanomaterials, significant problems with formulation processing occurs (Dokhan et al. 2002; Galfetti et al. 2007; Jiang et al. 2006). Propellants using nanomaterials often have poor mechanical properties and stability characteristics.

Another constraint that does not allow for the full potential of nanoparticle combustion is the effect of sintering (Chakraborty and Zachariah 2014) which is prevalent on the surface of burning solid propellant formulations leading to what has been traditionally called agglomeration. That is, as the burning front of the propellant exposes new particles on the burning surface they coalesce forming larger particles. The result is a larger particle that burns on a longer timescale than a nanoparticle would be expected to, and in the case of a solid propellant results in slag and two-phase flow loss. This concept has been shown both numerically (Chakraborty and Zachariah 2014) and experimentally (Egan et al. 2014).

Recently, researchers have created and studied nanocomposite microparticles using nanoaluminum bound within a polymer for various applications (Guerieri, DeLisio, Zachariah 2017; Huang et al. 2015; Jacob, Wei, Zachariah 2016; Wang et al. 2013, 2014, 2017; Young, Jacob, Zachariah 2015a). Wang et al. (2013) demonstrated that the ignition characteristics of nanocomposite microparticle thermites were equivalent to those of physically mixed nanothermites, while pressurization rates in a closed volume experiment were higher for the microparticles despite the particles being orders of magnitude larger. In a follow-on study, Wang et al. (2017) included ammonium perchlorate within a nanocomposite microparticle demonstrating a further reduction in particle ignition temperature of nearly 200 K below the aluminum melting point. Young, Jacob, Zachariah (2015a) replaced micrometer scale aluminum with nanocomposite aluminum NC structures in a composite solid propellant formulation resulting in a propellant burning rate increase of approximately 35%. Jacob, Wei, and Zachariah (2016) suggests that one of the main benefits of nanocomposite microparticles comprising neat nanoparticles is the inclusion of a gas generating binder, which helps to disassemble the particles into smaller fragments, and not allowing the particles to sinter. Ideally, these composite microparticles will improve formulation processing while still taking advantage of nanoscale reactivity.

This study investigates the ignition properties of nanocomposite structures of nanoaluminum, 1,3,5-trinitrohexahydro-s-triazine (RDX), and nitrocellulose (NC) formed by the electrospray technique. Aluminum is a common supplement to propellants and enhanced blast explosives due to its ability to enhance performance. Similarly, RDX is a common energetic ingredient in propellants and explosives. For the purposes of this study, NC is used as an energetic binder to create the composite structures. The composite

structures studied here offer an opportunity to evaluate synergistic effects that might offer pathways to new propellant and explosive formulations.

Methods/experimental

Materials

Nanostructured microparticles composed of aluminum (Al), RDX, and NC, were synthesized using a previously described electrospray deposition-based synthesis technique (Wang et al. 2013). Briefly, an electric field is applied between a needle and a substrate. A syringe pump delivers a precursor solution through the needle from which a Taylor Cone is formed, creating an aerosol plume. As the solvents evaporate, particles are formed and land on the substrate. In these experiments, a needle to substrate distance of 10 cm, a 2 kV/cm electric field, and flow rate of 1 mL/hour were employed. The electrosprayed composite was gently scraped off the collection substrate with a typical 2 mL precursor solution producing ~100 mg of dry powder. The Al nanopowder used in this work was purchased from Novacentrix with an active Al content of 81 mass%, determined by thermogravimetric analysis (TGA). The NC was purchased as a 4–8 wt. % collodion solution from Sigma-Aldrich. Ethanol, diethyl ether, and Dimethylformamide (DMF) were also purchased from Sigma-Aldrich. The RDX used in this study was RS-RDX from Eurenco and was dissolved in DMF at a loading of 95 mg/mL to create a stock solution for precursor preparation.

Four samples with varying Al:RDX ratios by mass of 1:3, 1:1, 3:1, and 9:1 (designated as Samples 1–4 respectively) were prepared, each containing a fixed amount of 5 wt. % NC as this amount of NC has shown the best performance in previously studied multicomponent electrospray synthesized microparticle systems (Wang et al. 2014). In constant volume experiments while varying the NC content in thermite microparticle composite formulations, Wang et al. (2014) found that 5 wt% NC resulted in the highest peak pressure and highest pressurization rate of all formulations studied. The microparticle composites also significantly outperformed physical mixtures of similar thermite mixtures. Similarly, Jacob, Wei, and Zachariah (2016) demonstrated enhanced combustion rates of nanoaluminum microparticles relative to as received nanoparticle aggregates in a flat flame burner experiment. In this study, although physical mixtures were not examined, we expect that similar performance enhancement would be observed relative to a physical mixture of the constituents due to the intimate mixing of the components and expected gas generation limiting the amount of agglomeration. A summary of the particles studied is shown in Table 1. To prepare the electrospray precursor solution, the dissolved RDX stock solution was added to the Al in a quantity that would achieve the desired Al:RDX mass ratio. NC was then added to this solution and the total volume was brought to 2 mL by adding 3:1 ethanol:diethyl ether. The solution was sonicated for 1 hour and then stirred for 24 hours prior to electrospraying.

Table 1. Summary of nanostructure microparticle composition.

Sample #	Wt% Al	Wt% RDX	Wt% NC
1	23.75	71.25	5
2	47.5	47.5	5
3	71.25	23.75	5
4	85.5	9.5	5

Both RDX and NC are nearly stoichiometrically balanced (slightly negative oxygen balance), meaning that they cannot act directly as oxidizers for the aluminum in the composite material. Each sample type considered is fuel rich. However, the combustion products of both RDX and NC, namely H_2O and CO_2 can act as an oxidizer for aluminum. In our case, none of the composite samples can produce enough H_2O or CO_2 to completely oxidize the remaining aluminum. For example, in our extreme case of the least amount of aluminum, using the NASA CEA Computer Code (McBride and Gordon 1996) we determined that after allowing the NC and RDX to react the mole fractions of H_2O and CO_2 are 0.160 and 0.064 respectively. The mole fraction of aluminum to react accounting for the oxide shell is 0.177. It requires 1.5x as much water vapor as aluminum in order to stoichiometrically consume the aluminum. Similarly, it requires 0.75x as much CO_2 as aluminum to consume all of the aluminum. In our other extreme case (most aluminum), after the consumption of NC and RDX, the mole fraction of H_2O and CO_2 remaining is 0.037 and 0.019 respectively, while the mole fraction of aluminum left to consume is 0.769.

SEM/XRD analysis

The Al/RDX/NC nanocomposites were first characterized using a Hitachi SU-70 FEG-SEM. Figure 1 provides representative images of each of the particles considered in this study. The particles with the highest RDX loading show the Al fully encased in a RDX/NC matrix. As the RDX loading in the precursor was decreased, the average particle diameter increased from ~ 500 nm to ~ 2 μm . The particles also became less spherical at the highest Al loading. X-Ray diffraction was also conducted on the samples showing crystalline RDX and aluminum within the composite particles as shown in Figure 2.

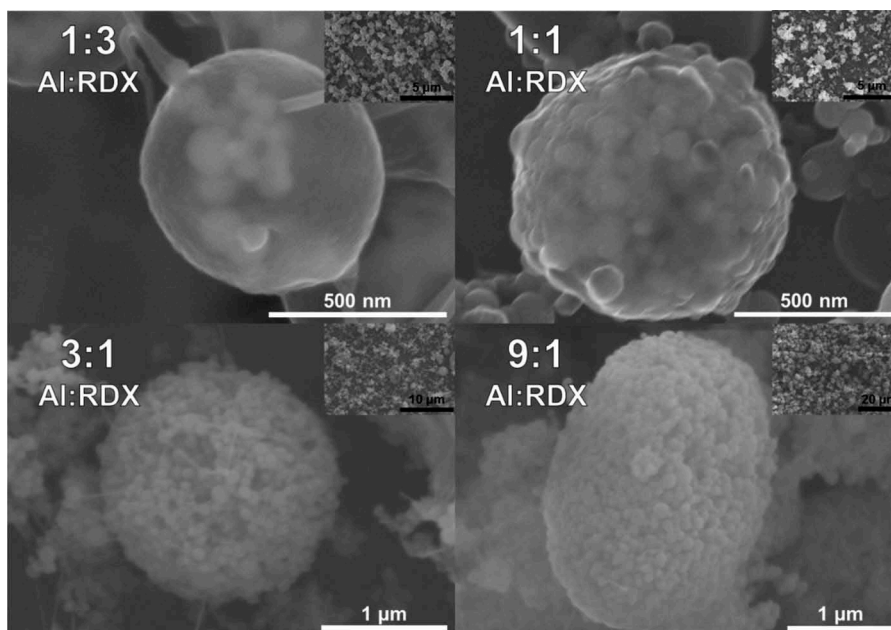


Figure 1. Scanning electron microscope images of Al/RDX/NC nanostructured microparticles.

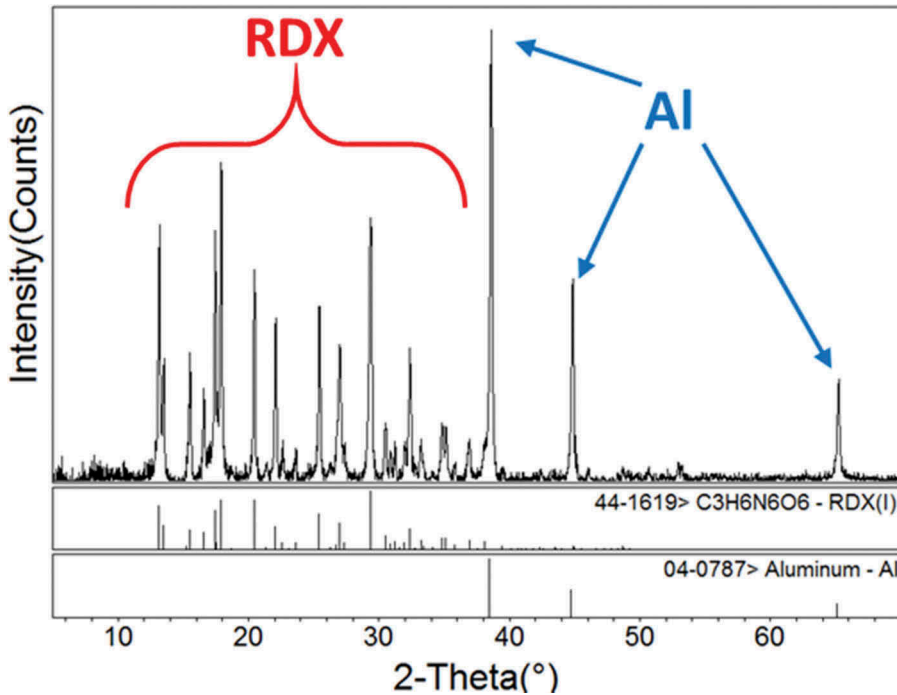


Figure 2. X-ray diffraction patterns for 1:3 Al:RDX.

Experiments

Two types of ignition experiments were conducted in this study. The first used our high pressure T-jump which has been described elsewhere (Young, Roberts, Stoltz 2015b; Young, Wang, Zachariah 2015c). Briefly, particles were deposited on a 75 μm platinum filament and placed in an optically accessible pressure vessel. The pressure vessel had three quartz windows available for observing the experiments. A voltage is quickly applied across the platinum filament causing it to be resistively heated, leading to an ignition event for a given sample. The heating rate used during the T-jump experiments in this study was approximately 100,000 K/s. During the experiments the platinum filament was heated from room temperature to in excess of 1000 K at which point any and all reactions that were expected would have been completed. Experiments were conducted with either air or nitrogen used as the pressurizing gas up to about 5.17 MPa. High speed videography was conducted using a Phantom 7.10 high speed camera to image the ignition events. Framing rates of 5000 frames per second and exposure times of 5 μs or 200 μs were used depending on whether or not any lighting was used to conduct shadowgraph imaging during the experiment. For shadowgraph imaging, a 250 Watt halogen light was used for backlighting the experiment. The reference time in the images, t_0 , refers to the first instance in which a reaction is detected in the video sequence.

For the second experiment, the high pressure T-jump was adapted for use as a laser ignition experiment by replacing the wire filament probe with a quartz window. Laser ignition experiments were conducted using a diode-pumped Nd:YAG (Lee Laser LDP200-MQ, CW, 1064 nm) laser with a nominal beam diameter of 3.8 mm and average photon

flux (on target) of 70 W/cm^2 . The power on target was held fixed for the entire study. The quartz window was purchased from National Quartz, and had a thickness of 19 mm and a transmission percentage of approximately 95% at the wavelength of interest. An external shutter (Uniblitz LS6Z2) was used to allow final light exposure and was opened by a user – controlled pulse generator (Stanford Research DG535). The shutter was opened for 250 ms and laser light was directed normal to the material surface the quartz window. Samples were loaded into a graphite fixture using $10 \pm 1 \text{ mg}$ for each experiment. Two Hamamatsu model H7827-012 photomultiplier tubes (PMT's) were used to monitor broadband light emission in real-time to characterize ignition, with the output sent directly to an oscilloscope. The PMT's had a spectral range of 300–850 nm, thus the laser pulse was not detected by the PMT's. During some experiments, an Ocean Optics USB 4000 Spectrometer replaced a PMT in order to determine species being formed during the ignition and combustion process. The spectrometer had a spectral range of about 200 nm to 530 nm. Experiments were conducted using air, nitrogen, or argon as the pressurizing gas with pressures up to 3.45 MPa. Figure 3 provides schematic diagrams of the two ignition experiments.

Results and discussion

High pressure t-jump

Initial ignition experiments were carried out using our high pressure T-jump. Figure 4 shows shadowgraph images of Sample 1 (Al:RDX = 1:3) during an ignition experiment at 0.101 MPa in air. In the shadowgraph images, dark structures surrounding the platinum filament are observed and are assumed to be the decomposition gases of the composite structure. Depending on heating rate, the decomposition of NC is expected to begin near $170 \text{ }^\circ\text{C}$ (Chen and Brill 1991; Hussain and Rees 1995), while RDX decomposition begins near $205 \text{ }^\circ\text{C}$. While there are many factors that can influence both NC and RDX decomposition onset, both would be expected to undergo decomposition and possibly deflagration at significantly lower temperatures than aluminum (Brzustowski and Glassman 1964; Friedman and Macek 1962, 1963) or nanoaluminum (Bazyn, Krier, Glumac 2007; Trunov et al. 2006) ignition. During this experiment, there was no clear evidence of aluminum ignition. Experiments were also carried out without backlighting and once again, there

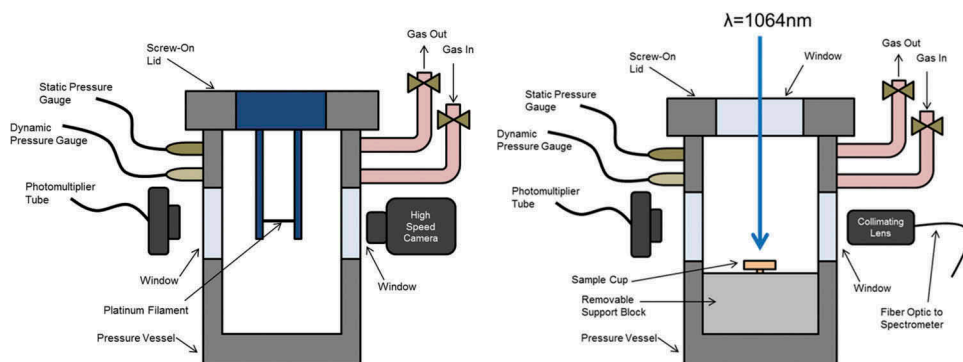


Figure 3. Schematic diagrams of (left) high pressure T-jump and (right) laser ignition experiments.

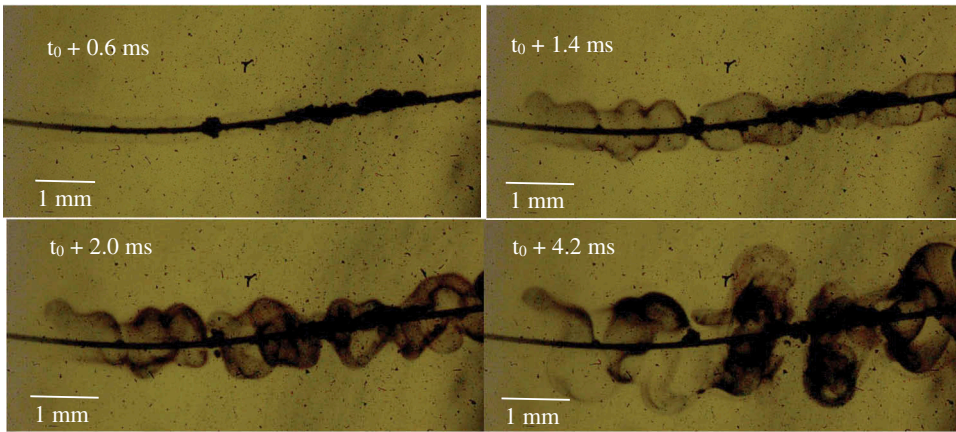


Figure 4. Shadowgraph Images of T-jump ignition of sample 1 at 0.101 MPa in air.

was no clear evidence of aluminum ignition, meaning that no significant particle or cloud luminosity was observed. The lack of luminosity also brings forth the question of whether or not the decomposition products of NC and RDX proceeded to deflagration, which cannot be confirmed by this experiment alone under these conditions. Under normal circumstances the platinum filament is heated in excess of the nanoaluminum ignition temperature. However, under atmospheric pressure conditions it appears that the decomposition products may have carried away the aluminum particles without igniting them.

Figures 5 and 6 show both shadowgraph and no lighting images of Sample 4 (Al: RDX = 9:1) T-jump ignition experiments at 0.101 MPa respectively. A density gradient can be seen in the shadowgraph image, which is likely to be the result of decomposition and possible deflagration of both RDX and NC in the mixture. The amount of RDX is significantly decreased in comparison to Sample 1 and therefore the amount of gas generated during decomposition is significantly less for Sample 4 resulting in a weaker density gradient in the shadowgraph images in comparison to Figure 4. In the no lighting condition, some evidence of aluminum ignition can be seen in the form of luminous particles leaving the platinum filament. As compared with Sample 1, with significantly less gas production and significantly more aluminum, the aluminum particles likely remained in proximity to the platinum heating filament for a greater duration resulting in ignition of the particles even if the NC or RDX did not proceed to deflagration.

Figure 7 shows the shadowgraph and images of Sample 1 during a T-Jump ignition experiment pressurized with air to 5.17 MPa. The shadowgraph images show very strong density gradients associated with the decomposition and deflagration of RDX and NC

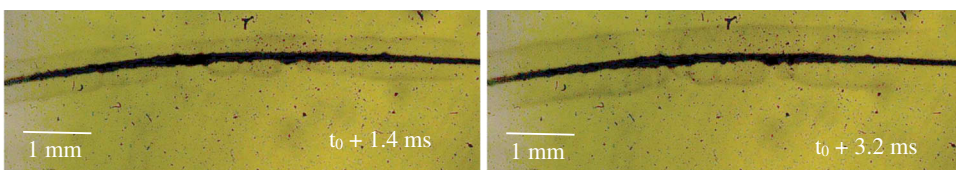


Figure 5. Shadowgraph Images of T-jump ignition of sample 4 at 0.101 MPa in air.



Figure 6. T-jump ignition of sample 4 at 0.101 MPa in air.

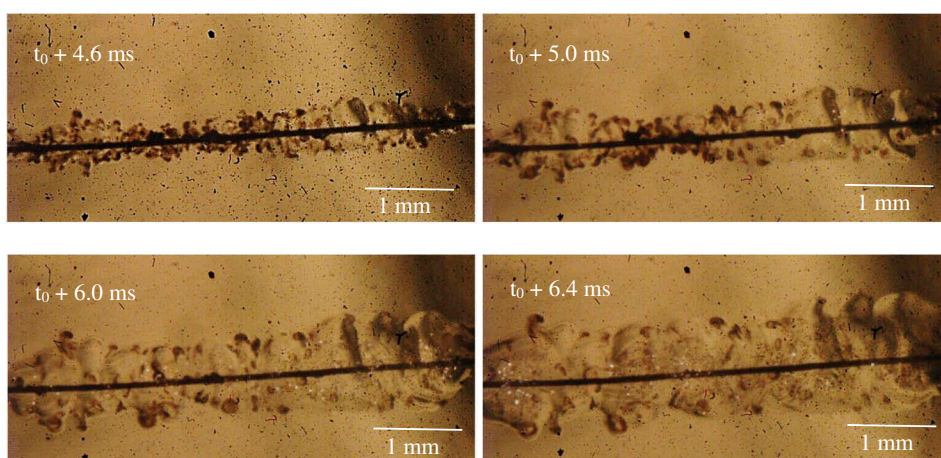


Figure 7. Shadowgraph images of T-jump ignition of sample 1 at 5 MPa in air.

relative to [Figure 4](#). The strength and propagation of the density gradients is a clear indication of the increased kinetic rates of combustion of RDX and NC. Additionally, luminous particles, assumed to be aluminum, can be seen within the boundaries of the density gradient. [Figure 8](#) provides representative images for Sample 1 during a T-jump experiment pressurized with air to 5.17 MPa with no additional lighting. During the no lighting conditions, very bright particles, assumed to be aluminum can clearly be seen to ignite and combust. These experiments were repeated in a nitrogen atmosphere to determine whether the aluminum was combusting aerobically or anaerobically with the combustion products of RDX and NC, which include species that could serve as an oxidizer for aluminum such as H_2O , CO_2 , NO , and NO_2 (Boggs 1984; Brill et al. 1992; Brill and Gongwer 1997; Chen and Brill 1991; Hussain and Rees 1995; Kim et al. 1997; Liau, Kim, Yang 2001; Makashir, Mahajan, Agrawal 1995). Water vapor and carbon dioxide in particular, commonly act as oxidizers for aluminum in solid rocket propellant combustion (Price 1984). During the experiments with nitrogen as the pressurant, similar gas phase structures could be seen in the backlit images indicating decomposition and combustion of RDX and NC, with some mild evidence of aluminum ignition observed as seen in [Figure 9](#). Each micro-particle is fuel rich, but this result does suggest that the combustion products of RDX and NC are responsible for the ignition of at least some of the aluminum in an anaerobic reaction.

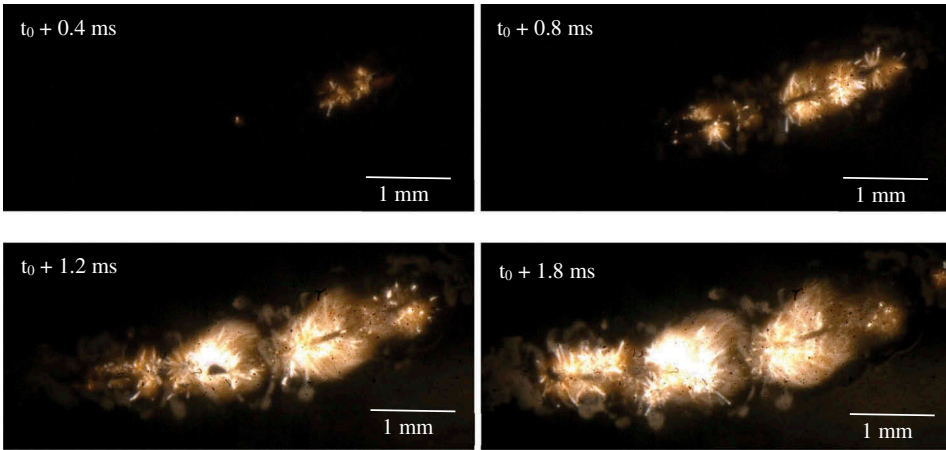


Figure 8. T-jump ignition of sample 1 at 5 MPa in air.

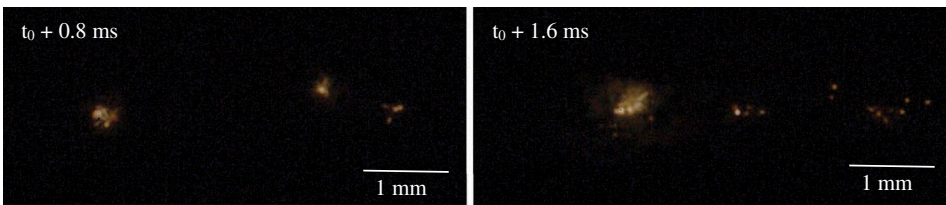


Figure 9. T-jump ignition of sample 1 at 5 MPa in nitrogen.

Figures 10 and 11 provides images of shadowgraph and no lighting T-Jump ignition experiments for Sample 4 pressurized with air to 5.17 MPa respectively. Due to the lower RDX content in comparison to Sample 1, the density gradients associated with

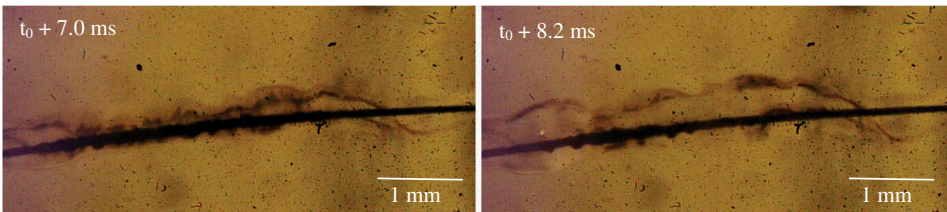


Figure 10. Shadowgraph images of T-jump ignition of sample 4 at 5 MPa in air.

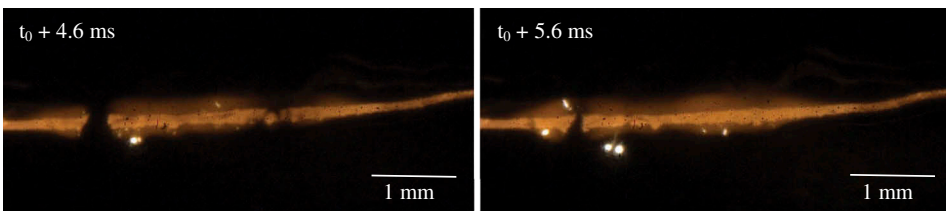


Figure 11. T-jump ignition of sample 4 at 5 MPa in air.

decomposition and combustion of RDX are weaker than those of Sample 1. Unlike Sample 1, for the no lighting condition of Sample 4, clear luminous ignition of aluminum is not obvious. However, we do observe a glowing phenomenon around the platinum filament previously unobserved for other samples or at other conditions. This may indicate aluminum ignition on or very near to the platinum filament as opposed to a dispersed ignition event as seen in [Figure 6](#). We speculate that this is due to the lower concentration of RDX in Sample 4 relative to Sample 1. We therefore hypothesize that the RDX serves as a gas generator, which can disperse the aluminum to its surroundings when in appropriate concentrations as in Sample 1. In the case of Sample 4 the concentration of RDX is not sufficient to disperse the aluminum particles and therefore they are confined to the region on or near the platinum filament. Furthermore, when comparing [Figures 8](#) and [11](#) it is clear that the combusting aluminum particle size in [Figure 8](#) (Sample 1) is smaller than those observed in [Figure 11](#) (Sample 4). The particles in [Figure 11](#) in particular on the order of 10's of micrometers. These results suggest that at low RDX content, the aluminum agglomerates to a much higher degree. Therefore, in applications where reaction time is critical, it may be important to include sufficient RDX in the composite material to minimize agglomeration.

During these experiments there are clearly competing reactions among the three reactants. As previously discussed, both RDX and NC ([Chen and Brill 1991](#); [Hussain and Rees 1995](#)) are expected to begin to react near 200 °C depending on the heating rate, while the nanoaluminum ([Bazyn, Krier, Glumac 2007](#)) would be expected to ignite near its melting point (660 °C). The primary visible light emitting reactant was aluminum, and in most cases any light emitted solely from NC/RDX decomposition/combustion was not significant enough to be recorded as an ignition event in our traditional detection system. In other words, the light output of the initial event could not be distinguished from the platinum filament heating. Therefore, in cases with the most aluminum, ignition temperatures would be biased to aluminum ignition temperatures. In cases with the least amount of aluminum, the aluminum was driven off of the platinum filament by the gas production from NC and RDX. The aluminum typically ignited in the products of NC and RDX and the surrounding oxidizing environment. All temperature measurements are normally based on filament conditions. However, in this case the local temperature due to combustion of RDX and NC may be very different from the filament. Thus, we can not accurately quantify the ignition temperature of the nanostructured microparticles in this experiment.

Laser ignition experiments

Laser ignition experiments were conducted over a pressure range of 0.101 MPa to 3.45 MPa using air, nitrogen, or argon as the pressurizing gas. Ignition delay was defined as the interval between the initial laser pulse and the first light detected by the PMT's. [Figure 12](#) provides an example of how the ignition delay was determined. [Figure 13](#) gives sample PMT traces for three different samples in air at 0.101 MPa demonstrating the difference in ignition delay between samples. The addition of aluminum to RDX serves to increase both the thermal conductivity and thermal diffusivity increasing the ignitability of the mixtures. The addition of aluminum also decreases the reflection coefficient of the mixture; however, for mixtures with more than 17% aluminum, it is only expected to be a weak influence at the wavelength of interest in this study ([Strakovskiy et al. 1998](#)). Therefore,

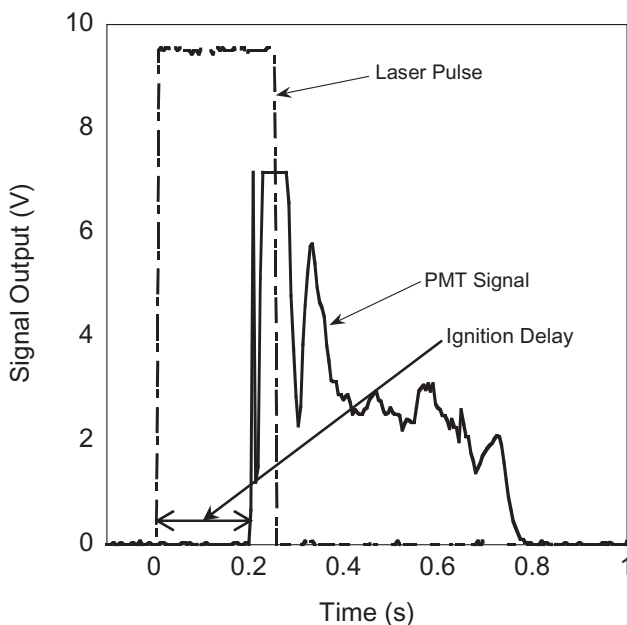


Figure 12. Example laser pulse and photomultiplier tube response indicating ignition of sample.

we believe that the difference in ignition delay between the samples is not simply an effect of absorptive properties alone.

Often in similar experiments, combustion times are extracted by using the light output of the reaction as collected here. In this study it would be reasonable to expect the composites with the largest amount of RDX to combust the quickest, especially at elevated pressure. However, inspection of [Figure 13](#) suggests the combustion times between samples may or may not follow the expected trend. In this case it is important to remember that our results are biased toward the reactants providing the brightest output during combustion, aluminum. Therefore, the light-based detection does not accurately capture RDX and NC consumption. The timescales observed during the experiment (100's of milliseconds) also indicate that we are resolving a propagation (with potential agglomeration) rather than anything resembling a single particle (Bazyn, Krier, Glumac 2007).

As [Figure 14](#) shows, all of the samples showed at least a slight decreasing trend in ignition delay as pressure was increased. In general, as the aluminum content in the particles increased there was less of a dependence of ignition delay on ambient pressure. Sample 1 had the longest ignition delay with delays of about 200 ms at 0.101 MPa which decreased to about 50 ms at 3.45 MPa. Sample 1 also had the greatest variability in ignition delay with some samples igniting well after the laser pulse. Therefore, only experiments when the sample ignited during the laser pulse are shown for Sample 1. Sample 3 had the lowest ignition delays ranging from 20 ms at 0.101 MPa to 15 ms at 3.45 MPa. Interestingly, the sample with the minimum ignition delay was a mixture that did not contain the least or the most amount of aluminum suggesting this is not the result of absorptive properties alone. If we consider the scanning electron microscope (SEM) images in [Figure 1](#) it allows us to speculate on potential ignition mechanisms. In the

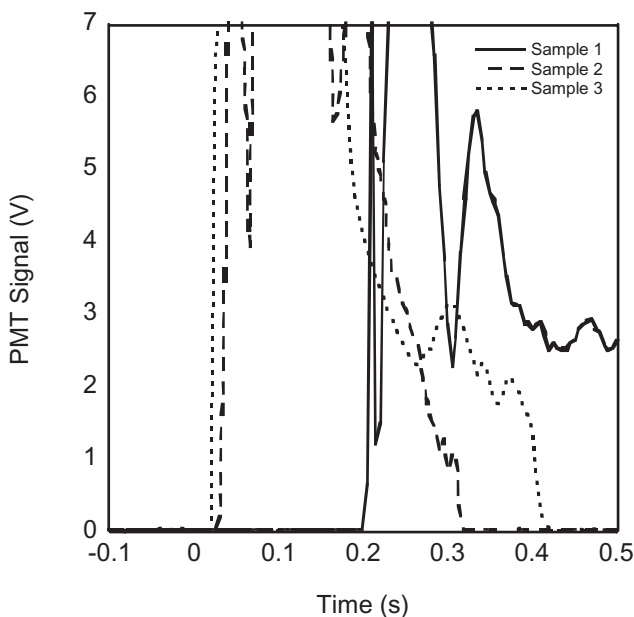


Figure 13. Ignition delay examples for various mixtures.

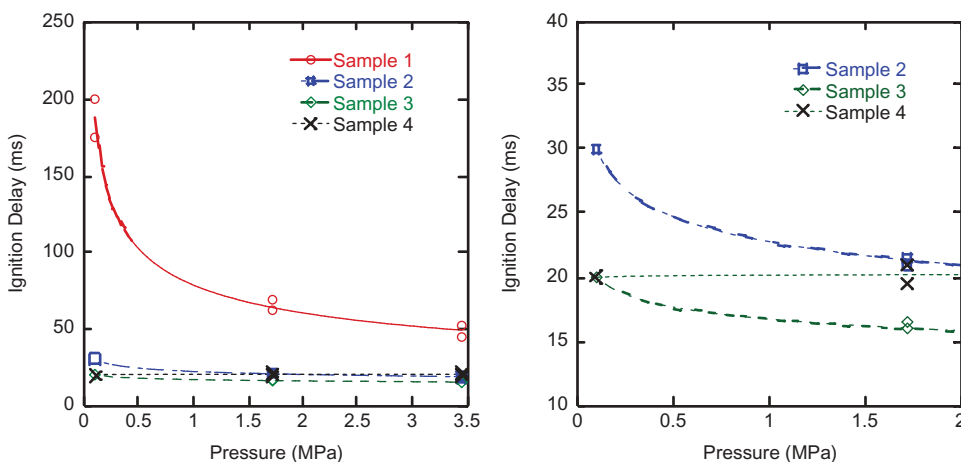


Figure 14. Ignition delay of microparticles as a function of pressure.

SEM image of Sample 1, the aluminum particles appear to be completely encapsulated by the RDX/NC mixture. The initial ignition of aluminum comes from the combustion products of RDX and NC, and therefore all of the surrounding RDX and NC must be removed to expose the aluminum for ignition. As more aluminum is added, less RDX and NC must be consumed in order to expose aluminum to the hot combustion gases and thus ignition delay decreases. Examining the most extreme case, Sample 4 which contains the most aluminum, the aluminum now begins to actively interfere with the decomposition and deflagration of RDX and NC which results in the ignition delay starting to increase

again. In addition, in the extreme case (most aluminum), the lower content of RDX and NC combustion products results in less heating of the aluminum particles.

Figure 15 shows the PMT traces for laser ignition experiments using Sample 3 in different environments; 1) air, 2) nitrogen, and 3) argon. As shown in the figure, the ignition delay is nearly identical for all three gaseous environments. This same result held true for all of the other samples as well. This suggests that the ignition process is not a function of environment, indicating that it is completely driven by mixture composition. This further implies that ignition of a given sample is driven by the decomposition/ignition process of RDX and NC. This result should not be surprising considering that both RDX and NC may behave as monopropellants and can supply all of the fuel and oxidizer to react without a supplemental oxidizer. In laser ignition studies on NC based propellants (Courty et al. 2018) and RDX based propellants (Gillard et al. 2018) also found that the environment was a non-influence on ignition delay. While the ignition process occurred at nearly the exact same time for each gas, the detected light intensity was much greater in air than in nitrogen or argon. In addition, the signal of the light detected in air appears to rise at a higher rate than those in the inert environments. Not surprisingly, this indicates that the combustion process is significantly aided by the oxygen available in air.

Emission spectroscopy was utilized to determine which species were being formed during the ignition and combustion event in three different atmospheres; 1) air, 2) nitrogen, and 3) argon. Figure 16 provides an example of the spectrum collected at 0.101 MPa. Several notable features are readily apparent in Figure 16. Atomic aluminum at 394 nm and 396 nm appear as well as AlO at 464, 484, and 509 nm. AlO is a commonly referenced gas phase intermediate during aluminum oxidation that is often used to identify a combustion event (Bucher et al. 1996). The spectrum shown in Figure 15 was collected in air, however there were no notable differences detected in nitrogen or argon. Since AlO was detected in both nitrogen and argon as well, this verifies that the aluminum at least partially reacts anaerobically with the combustion products of RDX and NC which

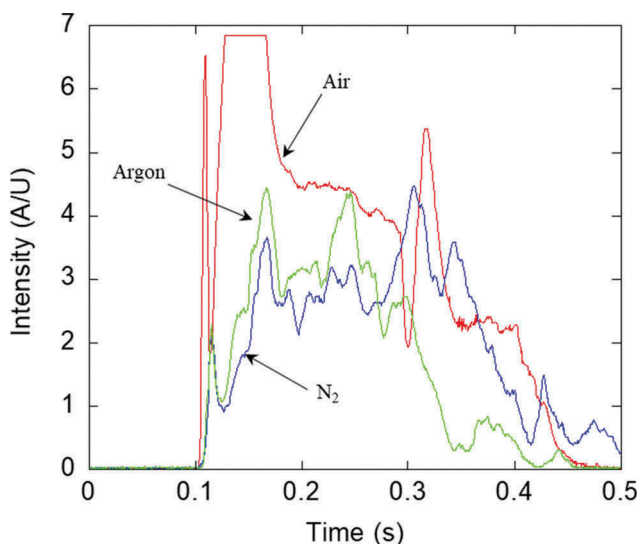


Figure 15. PMT signals for sample 3 in various environments at 0.101 MPa.

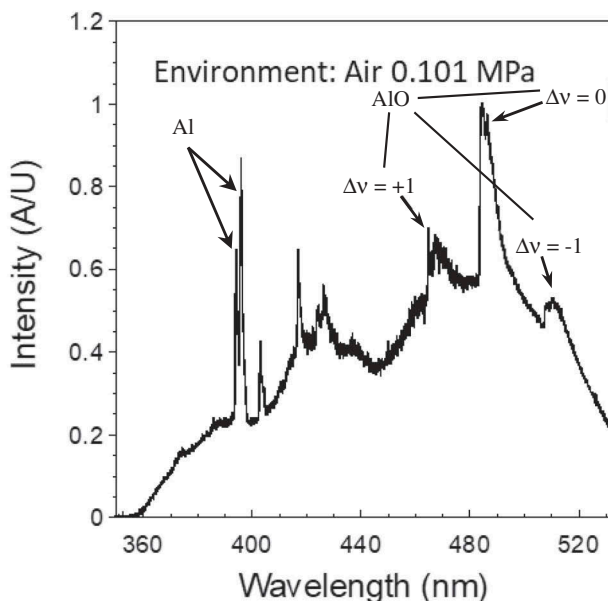


Figure 16. Emission spectra collected for sample 3 in air at 0.101 MPa.

include oxidizing species such as CO_2 , H_2O , NO , NO_2 , and N_2O . In earlier work, Mott Peuker et al. (2013) suggested that AlO emission may not be appropriate for identifying a combustion event when nano-scale particles are involved because it may not be a necessary requirement for aluminum combustion at these scales or that the source of AlO could come from Al_2O_3 thermal dissociation at high temperatures. However, as pointed out the composites in these studies were still plagued by agglomeration to some degree (see Figures 8 and 11) which we believe are the source of AlO emission. In the laser ignition studies where AlO was detected, the samples are placed as a powder into a cup where agglomeration would be far more likely to occur.

Conclusions

A high pressure T-Jump and a laser ignition experiment were used to study the ignition characteristics of Al/RDX/NC nanostructured microparticles. At low ambient pressure in the T-jump experiment RDX/NC decomposition was observed with minimal or no aluminum ignition. At high pressures, the RDX proved to be an efficient gas generator dispersing the aluminum and allowing it to combust with the ambient air particularly at lower aluminum loadings. Laser ignition experiments showed that the ignition delay decreased as the RDX content decreased to an optimum content. We believe this is the result of the differences in particle microstructure between samples. With low aluminum content, the ignition delay is limited to the time it takes to consume the RDX/NC mixture and release the aluminum. At very high aluminum loadings, the aluminum may interfere with RDX/NC combustion and begin to inhibit the aluminum ignition. This may be a balance between the hot gases released by RDX/NC combustion and heating/ignition of the aluminum particles. Laser ignition experiments in inert environments also verified that

the aluminum in all of the samples reacted at least partially anaerobically with the combustion products of RDX and NC via emission spectroscopy. In addition, the samples showed a decrease in ignition delay as the pressure increased likely due to the increase in RDX combustion kinetics with pressure.

Acknowledgments

The authors are grateful for the support of the Defense Threat Reduction Agency.

Funding

This work was supported by the Defense Threat Reduction Agency.

References

- Bazyn, T., H. Krier, and N. Glumac. 2007. Combustion of nanoaluminum at elevated pressure and temperature behind reflected shock waves. *Combust. Flame* 145:457–64.
- Boggs, T. L. 1984. The thermal behavior of cyclotrimethylenetrinitramine (RDX) and cyclotetramethylenetetranitramine (HMX). In *Fundamentals of Solid Propellant Combustion, Progress in Astronautics and Aeronautics*, ed. K. K. Kuo and M. Summerfield, vol. 90, 121–75. New York, NY: American Institute of Aeronautics and Astronautics.
- Brill, T. B., P. J. Brush, D. G. Patil, and J. K. Checn. 1992. Chemical pathways at a burning surface. *Proc. Comb. Instit.* 24:1907–14. doi:10.1016/S0082-0784(06)80224-9.
- Brill, T. B., and P. E. Gongwer. 1997. Thermal decomposition of energetic materials 69. Analysis of the kinetics of nitrocellulose. *Propellants Explos. Pyrotech.* 22:38–44. doi:10.1002/prep.19970220109.
- Brzustowski, T. A., and I. Glassman. 1964. Spectroscopic investigation of metal combustion. *Prog. Astronaut. Aeronaut.* 15:75.
- Bucher, P., R. A. Yetter, F. L. Dryer, T. P. Parr, D. M. Hanson-Parr, and E. P. Vicenzi. 1996. Flame structure of single, isolated aluminum particles burning in air. *Proc. Comb. Instit.* 26:1899–908. doi:10.1016/S0082-0784(96)80012-9.
- Chakraborty, P., and M. R. Zachariah. 2014. Do nanoenergetic particles remain nano-sized during combustion? *Combust. Flame* 161:1408–16. doi:10.1016/j.combustflame.2013.10.017.
- Chen, J. K., and T. B. Brill. 1991. Thermal decomposition of energetic materials 50. Kinetics and mechanism of nitrate ester polymers at high heating rates by SMATCH/FTIR spectroscopy. *Combust. Flame* 85:479–88. doi:10.1016/0010-2180(91)90149-6.
- Courty, L., J. F. Lagrange, P. Gillard, and C. Boulnois. 2018. Laser ignition of a low vulnerability propellant based on nitrocellulose: Effects of Ar and N₂ surrounding atmospheres. *Propellants Explos. Pyrotech.* 43:986–91. doi:10.1002/prep.201800087.
- Dokhan, A., E. W. Price, J. M. Seitzman, and R. K. Sigman. 2002. The effect of bimodal aluminum with ultrafine aluminum in the burning rates of solid propellants. *Proc. Combust. Inst.* 29:2939–45. doi:10.1016/S1540-7489(02)80359-5.
- Egan, G. C., K. T. Sullivan, T. LaGrange, B. W. Reed, and M. R. Zachariah. 2014. In situ imaging of ultra-fast loss of nanostructure in nanoparticle aggregates. *J Appl Phys* 115:084903. doi:10.1063/1.4867116.
- Friedman, R., and A. Macek. 1962. Ignition and combustion of aluminum particles in hot ambient gases. *Combust. Flame* 6:9–19. doi:10.1016/0010-2180(62)90062-7.
- Friedman, R., and A. Macek. 1963. Combustion studies of single aluminum particles. *Proc. Comb. Instit.* 9:703–09. doi:10.1016/S0082-0784(63)80078-8.

- Galfetti, L., L. DeLuca, F. Severini, G. Colombo, L. Meda, and G. Marra. 2007. Pre and post-burning analysis of nano-aluminized solid rocket propellants. *Aerosp. Sci. Technol.* 11:26–32. doi:10.1016/j.ast.2006.08.005.
- Gillard, P., L. Courty, S. De Persis, J. F. Lagrange, C. Boulnois, and I. Gokalp. 2018. Combustion properties of a low-vulnerability propellant: An experimental and theoretical study using laser ignition. *J. Energetic Mater.* 36 (3):362–74. doi:10.1080/07370652.2018.1439126.
- Guerieri, P. M., J. B. DeLisio, and M. R. Zachariah. 2017. Nanoaluminum/nitrocellulose micro-particle additive for burn enhancement of liquid fuels. *Combust. Flame* 176:220–28. doi:10.1016/j.combustflame.2016.10.011.
- Huang, C., G. Jian, J. B. DeLisio, H. Wang, and M. R. Zachariah. 2015. Electro spray deposition of energetic polymer nanocomposites with high mass particle loadings: A prelude to 3D printing of rocket motors. *Adv Eng Mater* 17 (1):95–101. doi:10.1002/adem.201400151.
- Hussain, G., and G. J. Rees. 1995. Thermal decomposition of RDX and mixtures. *Fuel* 74 (2):273–77. doi:10.1016/0016-2361(95)92665-S.
- Jacob, R. J., B. Wei, and M. R. Zachariah. 2016. Quantifying the enhanced combustion characteristics of electro spray assembled aluminum mesoparticles. *Combust. Flame* 163:281–89.
- Jiang, Z., S. F. Li, F. Q. Zhao, Z. R. Liu, C. M. Yin, Y. Luo, and S. W. Li. 2006. Research on the combustion properties of propellants with low content of nano metal powders. *Propellants Explos. Pyrotech.* 31:139–47. doi:10.1002/prep.200600021.
- Kim, E. S., H. S. Lee, C. F. Mallery, and S. T. Thynell. 1997. thermal decomposition studies of energetic materials using confined rapid thermolysis. *Combust. Flame* 110:239–55. doi:10.1016/S0010-2180(97)00062-X.
- Liau, Y. C., E. S. Kim, and V. Yang. 2001. A comprehensive analysis of laser-induced ignition of RDX monopropellant. *Combust. Flame* 126:1680–98. doi:10.1016/S0010-2180(01)00281-4.
- Makashir, P. S., R. R. Mahajan, and J. P. Agrawal. 1995. Studies on kinetics and mechanism of initial thermal decomposition of nitrocellulose, isothermal and non-isothermal techniques. *J. Therm. Anal.* 45:501–09. doi:10.1007/BF02548782.
- McBride, B. J., and S. Gordon. 1996. *Computer program for calculation of complex chemical equilibrium compositions and applications*. Washington, DC: NASA.
- Mott Peuker, J., P. Lynch, H. Krier, and N. Glumac. 2013. On alo emission spectroscopy as a diagnostic in energetic materials testing. *Propellants Explos. Pyrotech.* 38:577–85. doi:10.1002/prep.v38.4.
- Price, E. W. 1984. Combustion of metalized propellants. In *Fundamentals of solid propellant combustion, progress in astronautics and aeronautics*, ed. K. K. Kuo and M. Summerfield, Vol. 90, 479–513. New York, NY: American Institute for Aeronautics and Astronautics, Inc.
- Strakovskiy, L., A. Cohen, R. Fifer, R. Beyer, and B. Forch. 1998. Laser ignition of propellants and explosives. ARL-TR-1699, Aberdeen Proving Ground, MD: Army Research Laboratory. June.
- Trunov, M. A., S. M. Umbrajkar, M. Schoenitz, J. T. Mang, and E. L. Dreizen. 2006. Oxidation and Melting of Aluminum Nanopowders. *J. Phys. Chem. B* 110 (26):13094–99. doi:10.1021/jp0614188.
- Wang, H., R. J. Jacob, J. B. DeLisio, and M. R. Zachariah. 2017. Assembly and encapsulation of aluminum NP's within AP/NC matrix and their reactive properties. *Combust. Flame* 180:175–83. doi:10.1016/j.combustflame.2017.02.036.
- Wang, H., G. Jian, G. C. Egan, and M. R. Zachariah. 2014. Assembly and reactive properties of Al/CuO based nanothermite microparticles. *Combust. Flame* 161:2203–08. doi:10.1016/j.combustflame.2014.02.003.
- Wang, H., G. Jian, S. Yan, J. B. DeLisio, C. Huang, and M. R. Zachariah. 2013. Electro spray formation of gelled nano-aluminum microspheres with superior reactivity. *ACS Appl Mater Interfaces* 5:6797–801. doi:10.1021/am401238t.
- Young, G., R. Jacob, and M. R. Zachariah. 2015a. High pressure ignition and combustion of aluminum hydride. *Combust. Sci. Technol.* 187:1335–50. doi:10.1080/00102202.2015.1038383.

- Young, G., C. W. Roberts, and C. A. Stoltz. 2015b. Ignition and combustion enhancement of boron with polytetrafluoroethylene. *J. Propul. Power* 31:386–92. doi:[10.2514/1.B35390](https://doi.org/10.2514/1.B35390).
- Young, G., H. Wang, and M. R. Zachariah. 2015c. Application of nanoaluminum/nitrocellulose mesoparticles in composite solid rocket propellants. *Propellants Explos. Pyrotech.* 40 (3):413–18. doi:[10.1002/prop.v40.3](https://doi.org/10.1002/prop.v40.3).